京 都 大 学 防 災 研 究 所 年 報 第47号 C 平成16年3月
Annuals of Disas. Prev. Res. Inst., Kyoto Univ., No. 47 C, 2004

Long-period Ground Motion Simulation in Kinki Area

Nobuyuki YAMADA* and Tomotaka IWATA

* COE Researcher, DPRI, Kyoto University

Synopsis

We developed the crustal structure model from the source region of the Nankai trough to the Osaka basin in Kinki area for ground motion modeling by comparing observed records and simulated long-period (>2s) ground motions using finite difference method. We examined the records of an intermediate-size event (M_W4.3) and the largest aftershock (M_J7.0) of the 1946 Nankai earthquake occurred at the Nankai trough. The simulations of the S-wave part by a constructed 3D underground structure model reproduced well the observed records than the results by a simple 1D (flat layer) model. We showed that the 3D structure model is applicable for the ground motion simulation in the long period range, however it is needed more detail crustal velocity structure information for a better reproduction of the whole observed records.

Keywords: Long period ground motion simulation; Crustal structure model; Finite difference method; Kinki area

1. Introduction

Kinki area locates near the Nankai trough, which M8-class earthquakes have occurred repeatedly. The headquarters for earthquake promotion reported that long-term evaluations of occurrence potentials of the next earthquakes (Nankai and Tonankai) at the trough are from 40% to 50% within 30 years from 2001. Our recent mega-cities, such as Osaka, Kobe, and Kyoto cities, that have many large buildings, bridges, and oil tanks, have never experienced long-period ground motions by the M8-class large earthquake. Therefore, it is one of the important and urgent issues for the earthquake disaster prevention to predict long-period ground motions in the urban area during the hypothetical large earthquakes of the Nankai trough.

For accomplishing precise strong ground motion predictions, both of the source model and propagation-path underground structure model are needed (*e.g.* Kagawa *et al.*, 1998). Here we pay attention to construct the underground structure model. For the long-period ground motion estimation at the Osaka area for the large earthquakes of the Nankai trough, we need to construct a crustal model from the hypothetical source area to the Osaka basin. The Osaka basin was well investigated by many exploration surveys mainly after the 1995 Hyogo-ken Nanbu Earthquake, and a detail 3D basin model was constructed (*e.g.* Kagawa *et al.*, 2002). The constructed 3D basin model is confirmed by comparing between the synthetic and the observed ground motions (*e.g.* Zhao and Kagawa, 2002). On the contrary, the crustal structure model of outside the Osaka basin is not well examined. A simple 1D flat layer model has been used most of cases in the ground motion simulations.

In this study, we construct a 3D crustal model for ground motion simulations by referring to the previous studies. We also confirm the applicability of the model by comparing the observed ground motions and the synthetics in the long-period range (>2s) by finite difference method during the two earthquakes of M_W4.3 and M_J7.0 in Kinki area. Our aim of this study is shown in Fig. 1.

2. Underground Structure Model

Analysis area in this study is Kinki area of 220km(NS)×254km(EW), as shown in Fig. 2. This area includes mega-cities as Osaka and Kobe cities in the Osaka basin.

We prepared two underground structure models of the crust for this analysis. One is a 1D structure model. We referred the P-wave velocity model used at Wakayama observatory for the hypocenter determination (Nakamura *et al.*, 1997). S-wave velocity is assumed to be 1.0/1.73 times of P-wave velocity. We also assumed density and Q-values referred to the previous studies. This 1D P-wave velocity structure model and medium parameters are shown in Fig. 3a) and Table 1. We call this model '1D model'. The other is a 3D structure model. The each layer interface depth is referred to the depth contour maps of Conrad, Moho, and upper boundary of Philippine Sea plate (*e.g.*, Zhao *et al.*, 1994 and Furumura *et al.*, 2003). These contour maps are shown in Fig. 3b). This model also consists a surface flat layer with the thickness of 3km, which is the same as the surface layer of '1D model'. The medium parameters (Vp, Vs, and density) were referred to Shibutani (2001), as shown in Table 2. We assumed Q-values referred to the previous studies. We call this model '3D model'. Fig. 4 shows some profiles of the velocity structure models for '1D model' and '3D model'.

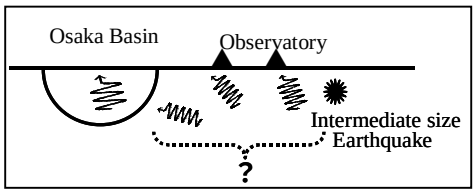

Fig. 1. Our aim is to confirm the applicability of the crustal structure model between the source region of the Nankai trough and the Osaka basin.

Table 1. Model parameters of '1D model'.

layer	ρ (g/cm³)	Vp (km/s)	Vs (km/s)	Q	depth (km)
1	2.50	5.50	3.17	400	0.0
2	2.70	6.00	3.47	600	3.0
3	2.80	6.80	3.93	700	15.0
4	3.20	7.90	4.57	1000	30.0
5	3.40	8.10	4.70	1500	75.0

Table 2. Model parameters of '3D model'.

layer	ρ (g/cm³)	Vp (km/s)	Vs (km/s)	Q	depth (km)
1	2.53	5.26	3.04	400	0.0
2	2.70	6.11	3.53	600	3.0
3	2.79	6.50	3.76	700	variable
4	3.29	8.10	4.50	1500	variable
5	3.16	7.74	4.30	1000	variable

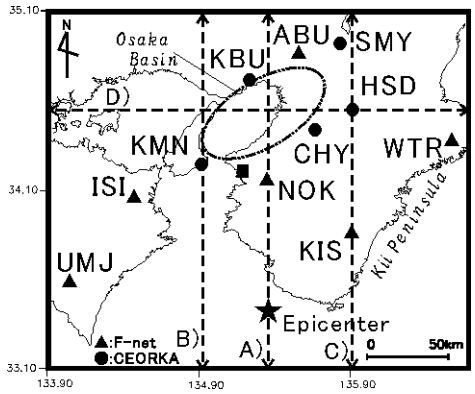

Fig.2. Map of analysis area. Triangles (F-net) and circles (CEORKA) are the locations of the rock site stations. Star and square show an epicenter of an earthquake M_W4.3 and the location of Wakayama observatory. Broken lines of A)~D) indicate the location of model profiles shown in Fig. 4.

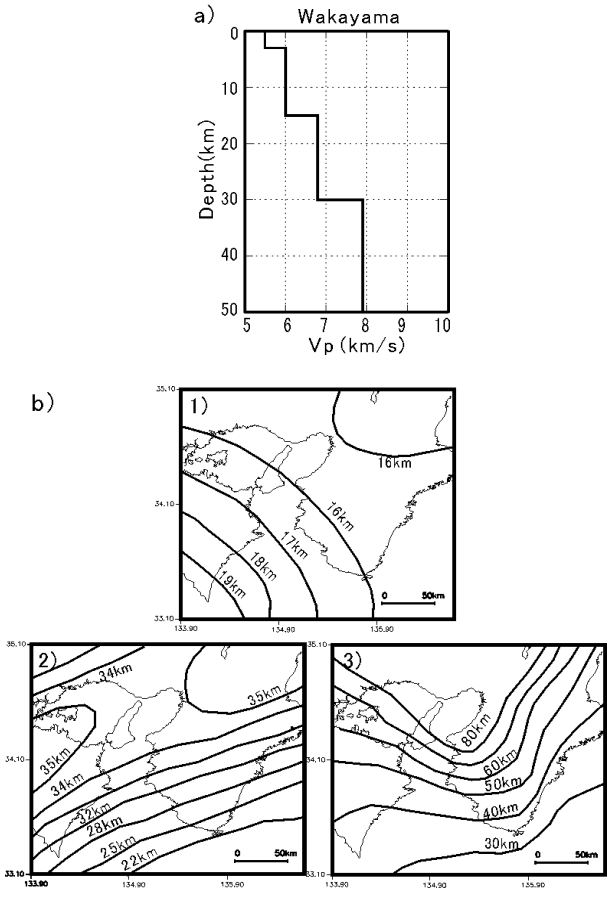

Fig. 3. (a) P-wave velocity profile for '1D model (Nakamura et al., 1997). (b) Contour maps of the boundary depth for '3D model'. 1) and 2) are Conrad and Moho discontinuity, respectively (Zhao *et al.*, 1994). 3) is upper boundary depth of Philippine Sea plate (Furumura *et al.*, 2003).

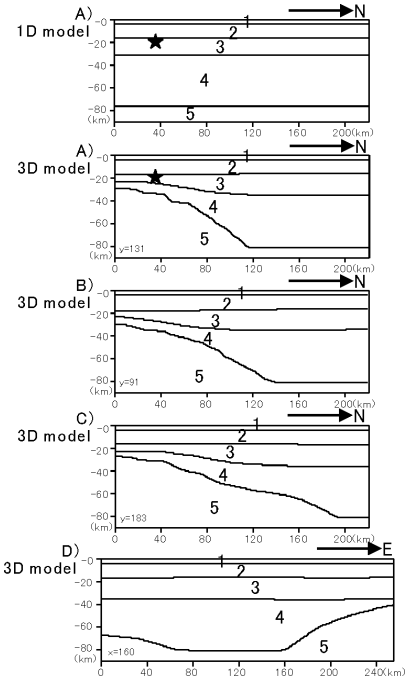

Fig. 4. Model profiles at the location of the broken lines of A)~D) in Fig. 2. Top figure is a profile of '1D model', the others are profiles of '3D model'. Profile A)s cross the hypocenter. Star shows the hypocenter of M_W4.3 event.

3. Long-period Ground Motion Simulation

We carried out the simulation of ground motions during an intermediate-size earthquake occurred in the source region of the Nankai trough using '1D model' and '3D model', and estimated which model is more applicable, by comparing observed ground motions and synthetics.

3.1 Observed Records of a M_W4.3 event

An intermediate-size earthquake of M_W4.3 occurred at south of Kii peninsula (33.41N, 135.33E, depth: 18km) was analyzed. The origin time is 21:14:21.8 on October 2, 2001 (J.S.T.). We used the source mechanism that is determined by F-net of National research Institute for Earth science and Disaster prevention (NIED). Fig. 5 shows the observed velocity records on the rock site of the stations by broadband seismogram network (F-net) of NIED and the Committee of Earthquake Observation and Research in the Kansai area (CEORKA), as shown in Fig. 2. Fig. 6 is Fourier amplitude spectra of the waveforms in Fig. 5 at five stations. These spectra are calculated for 40s after the S-wave onset in the waveform. We also estimated the noise level of 40s data length window that starts at 80s before the origin time at three stations of F-net. The amplitude spectra after the onset of S-wave in this figure show that the predominant period range is shorter than about 3s. The noise amplitude spectra show the peak around the period of 5s. These amplitudes before the event are equivalent to the amplitude after the onset at around the period of 5s. This indicates that S/N ratio is sufficient except for the period of about 5s for both horizontal components.

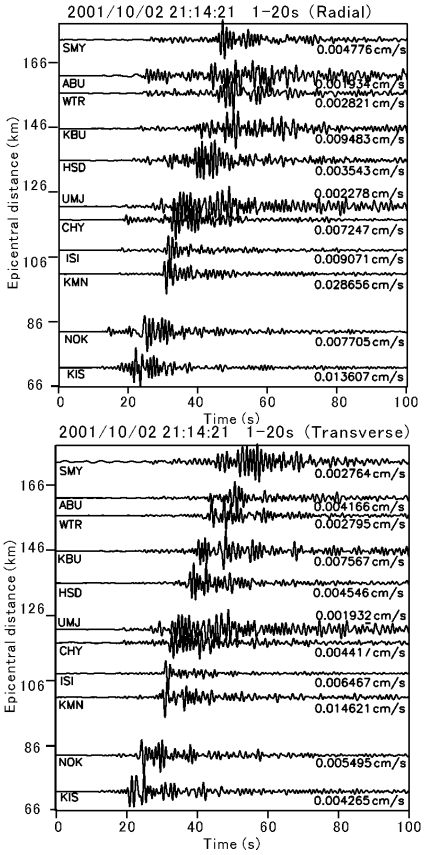

Fig. 5. Observed records of the target earthquake of October 2, 2001 on the rock sites in Fig. 2. These waveforms are radial and transverse components of long-period (1-20s) velocities. The number of right side of the waveforms is maximum amplitude in cm/s.

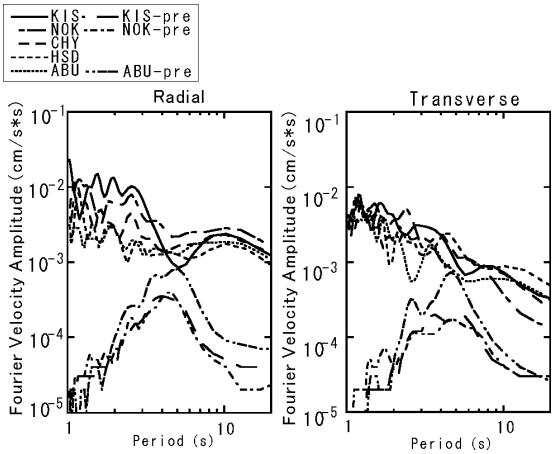

Fig. 6. Fourier velocity amplitude spectra of the waveforms for 40s after the S-wave onset at five stations and ones for 40s that is 80s before the origin time at three stations (KIS-, NOK- and ABU-pre) by F-net.

3.2 Finite Difference Simulation

The underground structure model is discretized with 1km grid spacing to resolve the minimum S-wave wavelength, in case of the fourth-order schemes (*e.g.*, Levander, 1988) which corresponds to the minimum resolved period of about 2s. The total nodes are 5.07 million in this simulation. Absorbing boundary (Clayton and Engquist, 1977) and a zone of attenuative material (Sochacki *et al.*, 1987) are applied to the sides of the computational model to mute the artificial boundary-generated waves. The medium attenuation formulation developed by Shimoyama and Koketsu (1997) in the medium is used, that is no distinction between Qp and Qs. The source is treated by adding the moment tensor in the finite difference grid (Graves, 1996). These finite difference simulation schemes in this study are developed by Yamada and Yamanaka (2001).

The source model of this earthquake is assumed to be a point source based on the information by F-net. The source time function is simple triangle pulse of 0.5s time window. This pulse width was determined by comparing the initial S-wave pulse width of the observed and synthetics. These parameters are listed in Tables 3 and 4.

3.3 Results of the Simulation

In this section, we showed the applicability of the models for ground motion simulation by comparing the observed and the synthetic ground motions by '1D model' and '3D model'. We analyzed the period ranges of 2-5s and 5-20s, because the S/N ratio is low at around the period of 5s, as shown in Fig. 6.

The comparisons of the observed waveforms and synthetic ones at five stations are shown in Fig. 7. In the period range of 2-5s, the direct S-wave part and its duration by '3D model' reproduce observed ones better than those by '1D model' at KIS, ISI and ABU. However, the synthetic durations of both models are much shorter than the observed one at HSD. From this result of that period range, the shallow crustal velocity structure model within several kilometers is thought to affect the ground motion characteristics. More detail information in the shallower part of the crustal structure is needed for getting the better fits.

In the period range of 5-20s, the results by '1D model' and '3D model' are almost same. The synthetic waveforms by the two models reproduce the observed records at ABU and HSD. However, the synthetics at KIS, NOK and ISI don't reproduce the observation. Although both models are different, we get similar synthetic waveforms. Therefore, we need to examine the source effects such as the source mechanism and south depth.

The comparisons of the observed maximum amplitudes and synthetic ones at all stations in the period range 2-5s and 5-20s are shown in Fig. 8. The maximum amplitudes (A) are estimated by the equation (1).

$$A = \sqrt{(RA)^2 + (TA)^2} \qquad (1)$$

RA and TA mean the maximum amplitudes of radial component and transverse component, respectively. In the period range of 2-5s, the maximum amplitudes from '3D model' are closer than those from '1D model' to observed ones at most of stations. The maximum amplitudes in the period range of 5-20s show the same tendency as the case of 2-5s period range, although the difference between the maximum amplitudes by '1D model' and '3D model' is very small.

As the other comparison, we estimated the group velocity from the source to the each station by picking up the peak time of the envelope waveforms. Fig. 9 shows the envelopes of observations and synthetics of horizontal components at five stations in the period range of 2-5s. The observed and synthetics group velocities in the period range 2-5s and 5-20s are listed Table 5. The group velocity values by '3D model' are closer to those of the observed than those by '1D model'.

These comparisons of the waveforms, maximum amplitudes, and group velocities, indicate that '3D model' is a better model for simulation of ground motions in the period range of 2-20s.

To see the spatial difference of waveforms between two models, we defined the difference $D(i,j)$ by the equation (2). $W1(i,j,k)$ and $W2(i,j,k)$ indicate the amplitude of the synthetic waveforms by '1D model' and '3D model', respectively. The i and j are spatial indices, and the k is a time index in the equation (2). We took the summation in the 30s window after the S-wave onset. The S-wave onset is estimated with assuming S-wave velocity of 4.5km/s. Fig. 10 shows the spatial distribution of the difference of the average of the three components of the $D(i,j)$ in the period range of 2-5s.

$$D(i,j) = \frac{\sum_k \{W1(i,j,k) - W2(i,j,k)\}^2}{\sqrt{\sum_k \{W1(i,j,k)\}^2}\sqrt{\sum_k \{W2(i,j,k)\}^2}} \qquad (2)$$

Generally, the difference is increasing with the epicentral distance. The large difference is observed in the area with the epicentral distance of about 100km. The differences between the synthetics seem to be occurred by the integration effects of the model difference from the source to observation sites.

Table 3. Simulation parameters.

Model area	NS:220km, EW:254km, Z:98km
Grid points	221×255×99
duration	100s
dx	1.0km

Table 4. Source parameters.

strike	N276 ° E
dip	72 °
rake	-75 °
M_0	3.49×10^{15}Nm
pulse width	0.5s
	point source

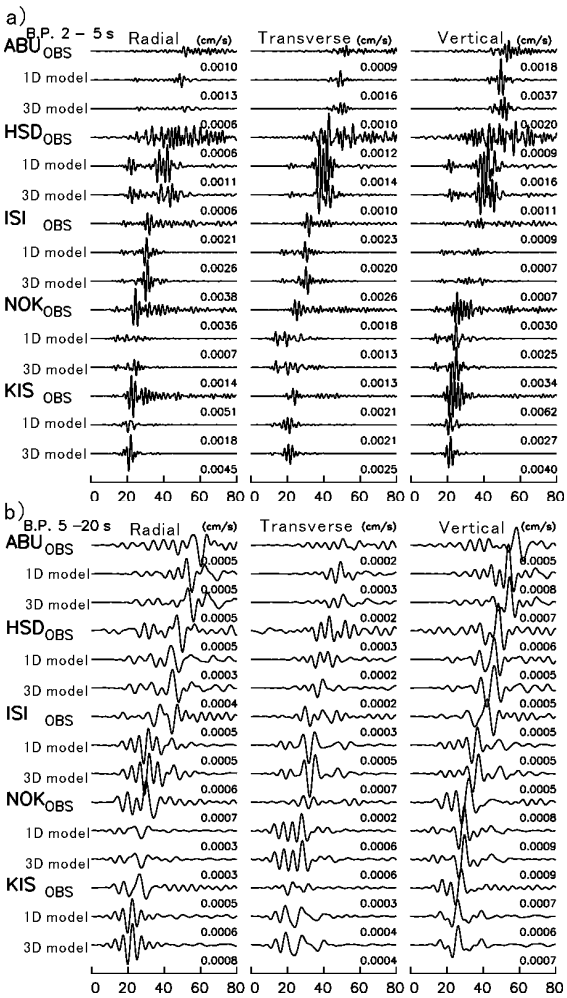

Fig. 7. Comparison of the observed waveforms and synthetic ones at five stations. (a) The period range of 2-5s. (b) The period range of 5-20s. Top waveform is observed, middle and bottom ones are synthetics by '1D model' and '3D model'. All waveforms are velocities. The lower right number of each trace is maximum amplitude in cm/s.

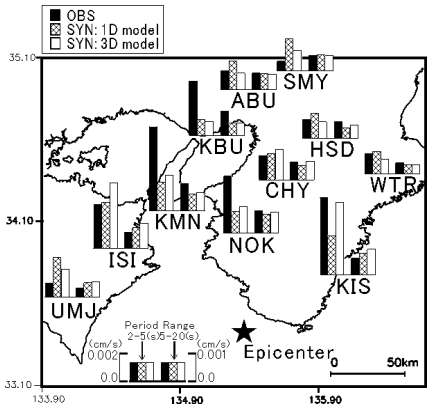

Fig. 8. Comparison of the maximum amplitude (A) of the observed and two synthetic motions all stations in Fig. 2. The left bars indicate the maximum amplitude in the period range of 2-5s, and the right bars indicate one in the period range of 5-20s.

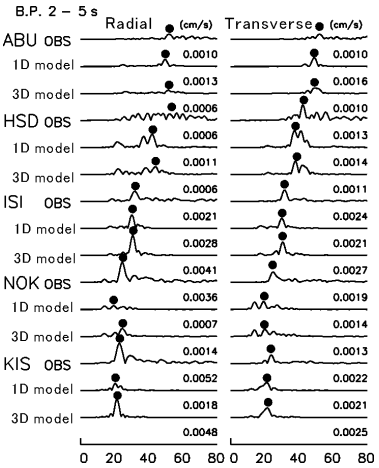

Fig. 9. Comparison of the envelope waveforms of observed and two synthetics of horizontal components. Black circles are peak point of the envelope waveforms in the period range of 2-5s.

Table 5. Lists of group velocity of observed data and synthetic one by '1D model' and '3D model' at five stations. Upper table is the period range of 2-5s and bottom table is the period range of 5-20s.

T:2-5s	delta	Radial comp.			Transverse comp.		
	(km)	OBS (km/s)	1D (km/s)	3D (km/s)	OBS (km/s)	1D (km/s)	3D (km/s)
ABU	161.9	3.11	3.26	3.14	3.10	3.30	3.28
HSD	135.8	2.41	3.23	3.09	3.20	3.61	3.57
ISI	108.1	3.39	3.57	3.52	3.41	3.59	3.53
NOK	83.0	3.38	4.25	3.38	3.33	4.27	4.12
KIS	71.9	3.15	3.51	3.35	3.01	3.38	3.33

T:5-20s	delta	Radial comp.			Transverse comp.		
	(km)	OBS (km/s)	1D (km/s)	3D (km/s)	OBS (km/s)	1D (km/s)	3D (km/s)
ABU	161.9	2.68	2.99	2.93	3.19	3.32	3.22
HSD	135.8	2.77	2.95	2.98	3.10	3.73	3.58
ISI	108.1	2.41	3.64	3.56	3.48	3.35	3.28
NOK	83.0	2.72	3.02	3.10	2.72	2.95	2.92
KIS	71.9	2.61	3.38	3.33	3.44	2.80	3.60

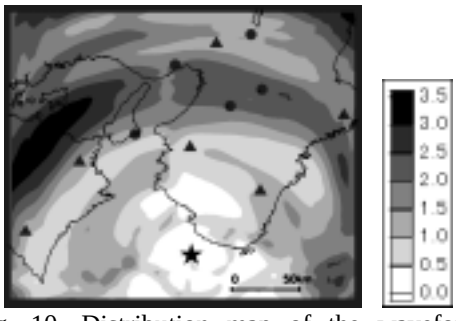

Fig. 10. Distribution map of the waveform difference (D) in the period range of 2-5s. Star indicates the location of epicenter. Circles and triangles are location of observatories of CEORKA and F-net.

4. Long-period Ground Motion Simulation during The Largest Aftershock (M_J7.0) of The 1946 Nankai Earthquake

In the previous chapter, we found that '3D model' was better for simulating ground motions of an intermediate-size earthquake (M_W4.3) in the period range of 2-20s. In Kinki area, there are no other records to examine the underground structure models in the longer period range, especially in the present broadband seismic network. We found a valuable record of the April 18, 1948 event (M_J7.0) at ABU, which is known as the largest aftershock of the 1946 Nankai earthquake. This record was observed by the strong motion seismograph and can be used for estimating the long period ground motions. Although there is only one station record, we could carry out the simulations during this event to examine the applicability of '3D model' as described in the previous chapter. Fig. 11 shows the location of epicenter, the focal mechanism (Iwata and Hamada, 1984), and some JMA observatories. As the observed waveforms at ABU (A triangle in Fig. 11) were recorded on smoked-paper, we had to digitize the records. We estimated the natural period and the damping ratio of seismographs using the response waveforms (Fig. 12). The natural period was estimated to 20.5s and 21.0s, the damping ratio was decided 0.50 and 0.41 for the NS component and the EW components, respectively. We convoluted these seismograph characteristics to synthetic waveforms. The numerical condition and underground structure models are the same in case of intermediate-size earthquake simulation. The source parameters are listed in Table 6 (Iwata and Hamada, 1984 and Ichikawa, 1971). Fig. 13 shows the result of the ground motion simulations at ABU. Although the absolute time of the observed record is not clear, the remarkable phase in the synthetic waveforms by '3D model' well reproduced the observed waveforms. This result suggests that '3D model' is appropriate for estimation of long-period ground motions. This kind of historical seismograms are found to be very useful for this kind of analysis.

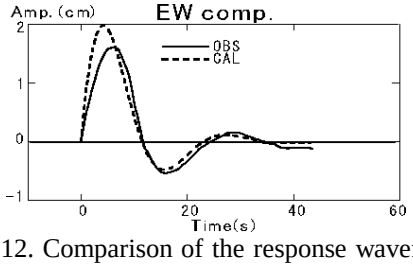

Fig. 12. Comparison of the response waveform (solid line) of EW component seismogram at ABU observatory and synthetic waveform (broken line) by the response of single degree-of freedom system with a natural period of 21.0s and a damping ratio of 0.41.

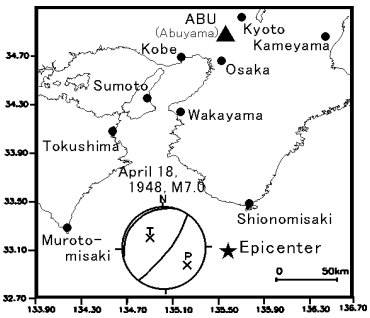

Fig. 11. Analysis area for the long-period ground motion simulation during the largest aftershock (M_J7.0) of the 1946 Nankai Earthquake. This figure shows the epicenter (star), focal mechanism and location of observatories of JMA (black circles). The triangle shows the location of ABU (Abuyama) observatory.

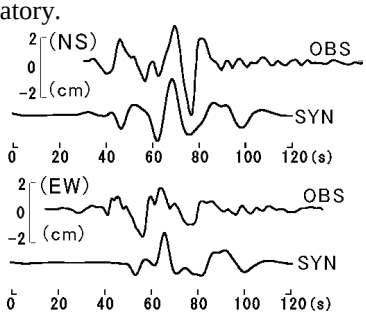

Fig. 13. Comparison of the waveforms between observed and synthetics. As the absolute time is not clear, these waveforms are fitted by the remarkable phase. The synthetics are well reproduced observed waveforms. The synthetics of NS component is convoluted to the seismograph characteristics with a natural period of 20.5s and a damping ratio of 0.50. The parameters of 21.0s and 0.41 are used for the EW component.

Table 6. Source parameters.
(Aftershock of the 1946 Nankai Earthquake)

epicenter	33.1N,135.6E
depth	27km
strike, dip, rake	N218E , 10, 90 (degree)
M_0	6.3×10^{19} Nm
	point source

5. Conclusions

We carried out some simulations of long-period ground motion and compared with observed records and synthetic results to estimate the validation of the crustal structure model in Kinki area. We constructed two crustal models, '1D model' and '3D model'. In case of the long-period ground motion simulation of an intermediate-size earthquake (M_W4.3), the synthetic ground motions by '3D model' were fairly agree with the observed ones at some stations in the period range of 2-20s, although there were poor reproductions at some stations. The other, validation of '3D model' in the longer-period range (about 20s) was also done with using the historical records of the largest aftershock (M_J7.0) of the 1946 Nankai

earthquake. To improve the fitting, we need information in the shallower crustal structure.

There was a regional characteristic in the spatial difference of waveforms between the two models. Large differences were appeared in the area of the epicentral distance of 100km, where the Osaka basin just exists. This implies that there is a possibility of influencing the simulation results of this period range by used underground structure model. It is important to construct more realistic underground structure model with model validations, as shown here, for the ground motion prediction in the longer period range.

Acknowledgments

The observed records were provided by NIED, CEORKA and ABU (Abuyama) observatory of Research Center for Earthquake Prediction, Kyoto University.

This research was supported by the Japanese Ministry of Education, Culture, Sports, Science and Technology (MEXT) 21st Century COE Program for DPRI, Kyoto University (No.14219301, Program Leader: Prof. Yoshiaki Kawata) as well as the Grant-in-Aid for Scientific Research (B) (1) (No. 15999999, Principal Investigator: S. Ikebuchi, Kyoto University). This manuscript partly follows the instructions given in IAHS Press (1995).

References

Clayton, R. and Engquist, B. (1977): Absorbing boundary conditions for acoustic and elastic wave equations, *Bull. Seism. Soc. Am.*, Vol. 67, 1529-1540.

Furumura, T., Kennett, B. L. N. and Koketsu, K. (2003): Visualization of 3D wave propagation from the 2000 Tottori-ken Seibu, Japan, Earthquake: Observation and numerical simulation, *Bull. Seism. Soc. Am.*, Vol. 93, pp. 870-881.

Graves, R. W. (1996). Simulating seismic wave propagation in 3D elastic media using staggered-grid finite differences, *Bull. Seism. Soc. Am.* Vol. 86, pp. 1091-1106.

Ichikawa, M. (1971): Reanalyses of mechanism of earthquakes which occurred in and near Japan, and statistical on the nodal plane solutions obtained, 1926-1968, *Geophys. Mag.*, Vol. 35, 207-274.

Iwata, T. and Hamada, N. (1986): Seismicity before and after the Tonankai Earthquake of 1944, *Zishin*, Vol. 39, pp. 621-634 (in Japanese).

Kagawa, T., Irikura, K., and Takemura, M. (1998): Estimation of strong ground motion -Present status and future-, *Zishin*, Vol. 51, pp. 339-454 (in Japanese).

Kagawa, T., Zhao, B., Miyakoshi, K. and Akazawa, T. (2002): A procedure of modeling basin structure used for strong ground motion evaluation from any amount of given information -Case study for the Osaka basin-, *The eleventh Japan earthquake engineering symposium*, pp. 497-500 (in Japanese).

Levander, A. R. (1988): Fourth-order finite-difference P-SV seismograms, *Geophysics*, Vol. 53, pp. 1425-1436.

Nakamura, M., Watanabe, H. Konomi, T. Kimura, S. and Miura, K. (1997): Characteristics activities of subcrustal earthquakes along the outer zone of southwestern Japan, *Annuals of DPRI*, Kyoto Univ., No. 40 B-1, pp. 1-20 (in Japanese).

Shibutani, T. (2001): *CHIKYU MONTHLY*, Vol. 23, No. 10, pp.708-713 (in Japanese).

Shimoyama, T. and Koketsu, K. (1997): Finite difference simulation of seismic ground motion in attenuative media, *Abstracts 1997 Japan Earth and Planetary Science Joint Meeting*, pp. 71 (in Japanese).

Sochacki, J., Kubichek, R., George, J., Fletcher, W. R. and Smithson, S. (1987): Absorbing boundary condition and surface waves, *Geophysics*, Vol. 52, pp. 60-71.

Yamada, N. and Yamanaka, H. (2001): Comparison of performance of 3D subsurface structural models in the southern part of the Kanto plain for strong ground motion –Examination using an earthquake (M_{JMA}4.1) in the west of Kanagawa prefecture of May 22, 1999-, *Zishin*, Vol. 53, pp. 313-324 (in Japanese).

Zhao, B. and Kagawa, T. (2002): Characterization of the Osaka basin model with high accuracy and its application –Strong motion simulation of the 2000 Tottoriken-Seibu Earthquake (M_{JMA}7.3)-, *The eleventh Japan earthquake engineering symposium*, pp. 501-504 (in Japanese).

Zhao, D., Hasegawa, A. and Kanamori, H. (1994): Deep structure of Japan subduction zone as derived from local, regional, and teleseismic events, *J. Geophys. Res.*, Vol. 99, pp. 22313-22329.

要　旨

近畿地方における南海トラフから大阪盆地に至る地殻構造モデルの妥当性の評価のために，紀伊半島沖で発生した２地震の周期２～２０秒のやや長周期地震動のシミュレーションを行った。用意した地下構造モデルは，平行層１次元モデルと既往の研究で示されていた地殻構造を３次元的にモデル化したものである。観測記録とシミュレーション結果を比較した結果、３次元構造が考慮されたモデルの方が観測記録をよく再現し、モデルが妥当なものであることを確認した。

キーワード：やや長周期の地震動シミュレーション，地殻構造モデル，差分法，近畿地方

COE-30

近畿地方における長周期地震動のシミュレーション

○山田伸之・岩田知孝

1. はじめに

南海トラフでの巨大地震の発生確率は 2001 年から今後 30 年以内に 40~50%と報告されている[地震調査推進本部(2001)]．巨大地震は，長周期地震動を強く発生させることに加え，大規模堆積盆地では長周期地震動が増幅伸長されることにより，堆積盆地上の都市は，周期数秒のやや長周期の地震動を強く受ける．都市圏に密集する超高層ビルなど長大構造物への長周期地震動の影響を定量的に評価することは，広域社会の安全を確保するために不可欠な要素である．

精度よい地震動評価のためには，詳細な震源と地下構造のモデルが必要である．後者については，南海トラフの巨大地震による京阪神地域における長周期地震動の高精度予測のために，震源域から大阪堆積盆地までの広域の地下構造情報が必要となる．1995 年兵庫県南部地震以降，大阪堆積盆地では多くの地下構造調査によって詳細な堆積層モデルが構築され，実地震記録を用いたモデルの妥当性の検証が始められているが，南海トラフの震源域から盆地に至る地殻構造については，実記録による検証が十分に行われていない．ここでは，既往の地下構造情報から地殻構造モデルを作成して，南海地震の震源域周辺の地震を対象としたやや長周期地震動のシミュレーションを行い，観測記録との比較からモデルの妥当性の検討を行った．

2. 中規模地震の地震動シミュレーション

対象領域は，四国東部から紀伊半島にかけての南北 220km 東西 254km とし，深さ方向は 98km とした．地殻構造モデルは，平行層モデル(Model 1)[中村･他(1997)]とモホ面やプレート上面などの深度分布図[例えば, Furumura(2003)]を参照に各面を媒質境界とするモデル(Model 2)を設定した．いずれのモデルも５層構造である．シミュレーションには，差分法を用い，格子間隔を 1km として，周期 2 秒以上を解析対象とした．

対象地震は，2001 年 10 月 2 日に発生した紀伊半島沖の地震(M_w4.3)である．シミュレーション結果は，防災科学技術研究所の広帯域地震観測網(F-net)および関西地震観測研究協議会(CEORKA)による岩盤観測点の記録と比較した．震源パラメータは，F-net で公表されている値を用い，点震源として設定した．ここでは，周期 2 秒～10 秒の周期帯域を対象にして, 観測波形と合成波形の比較を行った．これによると，Model 1 に比べて Model 2 の方が波形の形状や最大振幅など観測記録の特徴を表現できたと判断できる点が多く見られ，周期数秒の帯域では，現実的な広域地殻構造を地下構造モデルに取り入れる必要があることを表している．

3. やや規模の大きな地震の地震動シミュレーション

地下構造モデルの比較を行うために, 1948 年 4 月 18 日に紀伊半島沖で発生した地震(1946 年南海地震の最大余震 M_J7.0)の阿武山観測所の大震計記録の再現を試みる．観測記録は，煤書き記録をトレース後にデジタル化したものを用いた．震源位置等は，地震月報別冊第６号[気象庁(1982)]を参照にした．震源パラメータ等は，1946 年南海地震と同じ低角逆断層として，点震源を仮定した．Fig. 1 に，M_0=6.3×10^{19}Nm，時間幅 7 秒の三角波を震源時間関数とした場合の観測波形との比較を示す．比較のために合成波形は，地震計の特性を入れた変位応答波形にしている．ここでは，単純な震源時間関数を用いているため，今後詳細な検討が必要とする．いずれのモデルの結果もみかけ約 20 秒の周期の観測波形の特徴を示している．

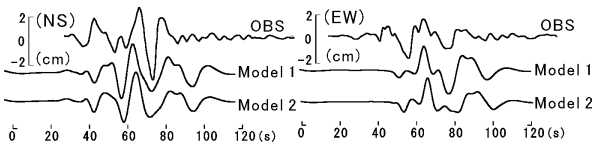

Fig.1. 阿武山観測所で得られた変位波形との比較．合成波形は，NS 成分で T_0=20.5s,h=50%, EW 成分で T_0=21.0s,h=41%とした変位応答波形．

謝辞:
地震予知観測研究センター阿武山観測所の浅田技官には，記録閲覧の便宜を図って頂きました．貴重な記録を保管されている関係諸氏に感謝致します．